Ab initio study of spin-orbit coupling effects on the low-lying excited states of NiO

K. Satitkovitchai, Y. Pavlyukh, and W. Hübner
Department of Physics, Kaiserslautern University of Technology, Box 3049, D-67653, Kaiserslautern, Germany
(Received 13 September 2004; revised manuscript received 21 April 2005; published 13 July 2005)

We show the results of *ab initio* embedded cluster calculations of the ground state and low-lying excited states of the (001) surface and bulk of NiO including the spin-orbit coupling effects. The calculations are performed by the COLUMBUS package using the combination of the relativistic effective core potentials and the spin-orbit operators. These effects result in the splitting of the *d-d* excited states. The fine structure of the $3d^8$ levels of the Ni^{2+} ion in NiO bulk and its (001) surface is resolved yielding good agreement with experimentally observed second-harmonic and optical absorption spectra. In addition, we discuss the transition electric-dipole moments, which can be used for a quantitative comparison with the experimentally determined optical intensities as well as for the exploration of various ultrafast all-optical spin-switching scenarios.

DOI: 10.1103/PhysRevB.72.045116 PACS number(s): 72.80.Ga, 71.15.Qe, 42.65.An, 31.15.Ar

I. INTRODUCTION

Magnetic and optical properties of transition metal oxides (TMOs) are governed by the ground state and low-energy excitation spectrum of the *d* shell of the central transition metal (TM) ion. These spectra have successfully been fitted to crystal field theory.[1] It is the strong Coulomb interaction between the 3*d* electrons that leads to an energy splitting of the d^n and d^{n+1} states. All *d-d* transitions violate the Laporte[2] orbital selection rule ($\Delta l = \pm 1$). Consequently, the low-lying excited states, so-called dipole-forbidden *d-d* transitions, appear as weak features in optical spectra. For the earlier work, Newman and Chrenko measured the *d-d* transitions in bulk NiO by using absorption spectroscopy.[3] Only recently, reliable experimental data have become available for *d-d* transitions of the bulk and (001) surface of NiO.[4–9] These results covered a range of 0.5–3.0 eV by means of electron energy-loss spectroscopy (EELS). The multiplicity-conserving ($\Delta S = 0$), as well as multiplicity-changing transitions ($\Delta S = \pm 1$), are easily observable with EELS if a suitable energy of the incident electrons is chosen.[10] It has been supposed that the intensity of triplet-singlet *d-d* transitions in NiO depends on the antiferromagnetic ordering of the magnetic moments,[11–13] yet an investigation of *d-d* transitions above the Néel temperature has not been reported.

The calculated *d-d* excitation energies of the bulk and (001) surface of NiO were investigated at the first-principles unrestricted Hartree–Fock level of theory by Mackrodt and Noguera.[14] These results allow for comparisons with optical absorption and EELS and with the theoretical works based on first-principles multireference coupled electron pair approximations (CEPA)[4] and complete active space self-consistent field theory–complete active space second-order perturbation theory (CASSCF/CASPT2)[15,16] calculations of embedded clusters of the type $(NiO_6)^{10-}$ for the bulk and $(NiO_5)^{8-}$ for the (001) surface of NiO, respectively. From the results of these calculations, which have included electron correlation in different ways and at different levels of sophistication, it has been concluded[4,15,16] that the inclusion of electron correlation effects is an essential prerequisite for an accurate description of *d-d* excitations in NiO.

In a previous study,[17] we have developed an *ab initio* theory for the second harmonic generation (SHG) from the NiO(001) surface. Our SHG spectrum for the (001) surface of NiO can be compared with experiment providing an alternative explanation of detecting SHG signal. In order to achieve this purpose we have two main implications: first, we investigated the electronic excitations of NiO by means of *ab initio* calculations. Thus, we have performed QCISD(T) calculations for the ground state and *d-d* transitions of NiO and compared them with the available experimental and theoretical data. Second, we computed the nonlinear optical response of the NiO(001) surface by using many-body wave functions and energies from the earlier work assignment.[17] However, we realized that, for the optical spin manipulation and nonlinear magneto-optics, it is important to include spin-orbit coupling (SOC) in the electronic theory.

This is a most important aspect of the present work. Since the high quality linear and nonlinear (SHG) optical spectra of NiO by Fiebig *et al.*[18] became available, it is possible to directly compare the experimental and theoretical details of the fine structure. An additional effect of splitting of the electron energy levels results from the spin-orbit coupling, which is characterized by the interaction between the electron spin moment and the orbital angular momentum, gives origin to a multitude of complicated physical phenomena, of which the magnetic anisotropy is a typical representative. A qualitative explanation by Van Vleck[19] of the magnetic anisotropy as an interplay between the dipole-dipole coupling between the spins and the spin-orbit coupling, and a subsequent theory by Brooks[20] on the anisotropy in itinerant ferromagnets emphasized the role of this relativistic effect already more than 6 decades ago. In this work we will therefore present the results of *ab initio* embedded cluster calculations for the ground state and low-lying excited states such as *d-d* transitions of the (001) surface and bulk of NiO including the spin-orbit coupling effects. These effects were taken into account by using the configuration interaction singlet (CIS) method including relativistic effective core potential (RECP) and spin-orbit operators, which is implemented in the COLUMBUS program. From this calculation, the fine structure splitting due to spin-orbit coupling effects is identified and

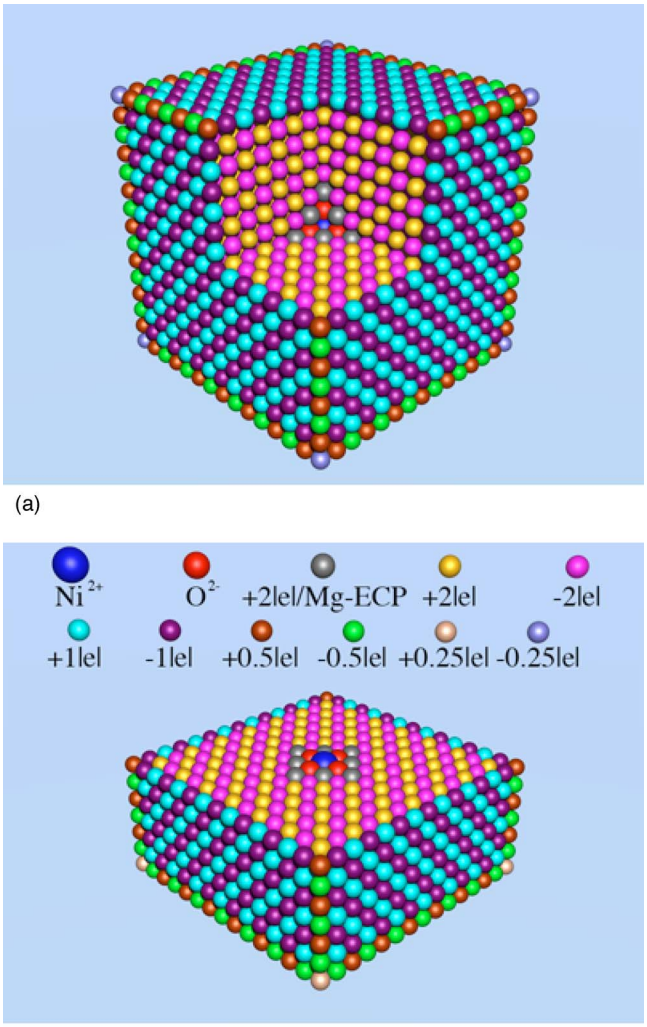

FIG. 1. (Color online) The embedded $(NiO_6)^{10-}$ and $(NiO_5)^{8-}$ clusters modeling a) the bulk and b) the (001) surface of NiO.

compared to the experiment.[18] Excellent agreement for bulk NiO is found. Finally, we determine the possible transition electric-dipole (ED) moments corresponding to the experimental oscillator strength.

II. COMPUTATIONAL DETAILS

A. Embedded cluster model

The smallest suitable cluster to simulate bulk NiO consists of one Ni ion and six nearest-neighbor O ions forming a cubic crystallographic arrangement in the point group O_h $(NiO_6)^{10-}$. The NiO(001) surface is represented by a $(NiO_5)^{8-}$ cluster of C_{4v} point group symmetry.[21] The length of the Ni—O bond has been fixed at 2.0842 Å according to experimental data.[22]

In order to correctly account for the electrostatic environment due to the rest of the ionic solid crystal, we embed the bare clusters in a set of point charges located at the lattice sites (Fig. 1). The point charges at the edges of the calculated slabs are fractional. In the vicinity of the quantum cluster, the point charges were exchanged by effective core potentials (ECPs) with the total charge +2; for that purpose we used magnesium cores $1s^2 2s^2 2p^6$ deprived of 2 valence electrons in order to simulate Ni^{2+} ions. This allows for the proper description of the Pauli repulsion within the cluster and the nearest-neighbor point charges and prevents a flow of electrons from oxygen ions to the point charges. Our analysis shows the convergence of the results with cluster sizes of $15\times15\times15$ point charges for bulk NiO and $15\times15\times7$ point charges for the NiO(001) surface. As a basis set for the Ni^{2+} ion, we use the ECP and corresponding $(8s,5p,5d)/[3s,3p,2d]$ basis set in valence double-zeta contraction (Lanl2DZ: Los Alamos ECP plus double zeta on Ni),[23] while for the oxygen a $(11s,5p,1d)/[4s,3p,1d]$ basis set with diffuse function was selected $(6-31+G^*$, Refs. 24–26).

B. Treatment of spin-orbit coupling

The atomic nonrelativistic Hamiltonian does not involve electron spin. In reality, the existence of spin adds an additional term (usually small) to the Hamiltonian. This term, called the spin-orbit interaction, breaks spin rotation invariance and thus lifts the degeneracy of atomic levels (fine structure splitting). Spin-orbit interaction is a relativistic effect and is properly derived using Dirac's relativistic treatment of the electron as

$$\hat{H}^{SO} = \xi(r)\vec{l}\cdot\vec{s}, \tag{1}$$

where $\xi(r)$ is

$$-\frac{e\hbar^2}{2m^2c^2}\frac{1}{r}\frac{dU(r)}{dr} \tag{2}$$

with a spherically symmetric potential $U(r)$ for the electron.

For relativistic quantum chemical methods, the analytical inclusion of spin-orbit interaction is now routinely available for HF, MC-SCF, and CI wave functions. Additionally, the inclusion of spin-orbit coupling has been successfully implemented in the Møller–Plesset perturbation theory as well as within the CC method. As mentioned, relativistic effects can be characterized by a variety of ways. Here, for the underlying theory of spin-orbit coupling effects we refer to the literature.[27,28]

In recent years, Pitzer *et al.*[27] have proposed a technique for calculating the spin-orbit interaction energy by means of spin-orbit configuration interaction. This method is obtained by the graphic unitary group approach (GUGA) in combination with relativistic core potential and spin-orbit operators, thus providing an efficient way for treating the electronic structure of molecules containing heavy atoms. The development of the spin-orbit matrix elements and the implementation of these methods in the COLUMBUS[29–32] suite of programs will briefly be described below.

The RECP and SO operator represent, for the valence electrons, the repulsion of the core electrons, the spin-orbit interaction with the nucleus, the spin-orbit interaction with the core electrons, and an approximation to the spin-orbit interaction between the valence electrons,[33] especially for heavier element systems.

The potential obtained from relativistic atomic wave functions is given by

$$\hat{U}^{REP} = \sum_{l=0}^{\infty} \sum_{j=|l-1/2|}^{|l+1/2|} U_{lj}^{REP}(r)\hat{O}_{lj}, \tag{3}$$

where REP denotes the relativistic effective potential, and the $\hat{O}_{lj}$ are (spin-dependent) projection operators and given as

$$\hat{O}_{lj} = \sum_{m=-j}^{j} |ljm\rangle\langle ljm|. \tag{4}$$

The REP operators can be expressed in a more readily usable form in terms of the spin-independent projection operators $\hat{O}_l = \Sigma_{m=-l}^{l} |lm\rangle\langle lm| = \Sigma_j \hat{O}_{lj}$,

$$\hat{U}^{REP} = \sum_{l=0}^{\infty} U_l^{AREP}(r)\hat{O}_l + \sum_{l=1}^{\infty} \xi_l(r)\vec{l}\cdot\vec{s}\hat{O}_l = \hat{U}^{AREP} + \hat{H}^{SO}, \tag{5}$$

where $U_l^{AREP}(r)$ is an averaged relativistic effective potential and $\xi_l(r)$ depends on the difference of $U_{l,l+1/2}(r)$ and $U_{l,l-1/2}(r)$. These two terms are readily identified[34,35] as core potentials and spin-orbit operators, respectively. The $U_l^{AREP}(r)$ are approximately independent of l when $l \geqslant L$, where L is larger by one than the largest l value of the core electrons. Then U^{AREP} can be reduced to

$$\hat{U}^{AREP} = U_L^{AREP}(r) + \sum_{l=0}^{L-1} [U_l^{AREP}(r) - U_L^{AREP}(r)]\hat{O}_l. \tag{6}$$

The spin-orbit operator has a form

$$\hat{H}^{SO} = \sum_{l=1}^{L} \xi_l(r)\vec{l}\cdot\vec{s}\hat{O}_l. \tag{7}$$

With these forms, existing programs for nonrelativistic calculations can be adapted to include relativistic effects. The additional integrals of U^{AREP} and H^{SO} are included in the COLUMBUS programs.

According to the outlined above prescription of the treatment of the relativistic effects the work is organized as follows.

- We compute singlet and triplet excited states of the bulk and (001) surface of NiO system within the CIS framework excluding SO coupling effects.
- Furthermore, in order to facilitate symmetry classification of the fine-structure levels we consider the theory of the splitting of atomic energy levels in the crystalline field including the effects of spin-orbit coupling, by following a paper by Cracknell.[36] We demonstrate how crystal field and spin-orbit splittings can be obtained from a unified point of view by subducing the direct product of angular momentum and spin representations over the irreducible representations.
- Then, we use the GUGA-CI programs in the COLUMBUS code for multireference singles CI calculations including the spin-orbit interaction operators and the RECP (Ref. 27) in order to obtain fine structure of the *d-d* transitions. We discuss singlet-triplet mixing and the electric-dipole transition moments among the states.

Although the inclusion of electron correlations weakly affects the spin-orbit splitting, it is interesting to repeat the relativistic calculations on the CISD or higher level of theory. This would be the subject of a forthcoming work. It should be mentioned here that for NiO (with two holes in the *d* shell) the inclusion of single and double excitations from the reference wave function already leads to a large improvement of the electron correlation by coupling the two-hole configurations in the 3*d* shell. However, this means that a higher level of theory such as QCISD(T) method just serves as a basis for a small correction to CISD approach.

III. RESULTS AND DISCUSSION

A. Inclusion of spin-orbit coupling

1. Symmetry analysis

In our theoretical study of NiO, we concentrate on the 21 lowest triplet states originating from the crystal field and spin-orbit splitting of the ^3F level of the Ni^{2+} ion. These states result from the distribution of eight electrons over ten spin orbitals. According to the prescription of group theory, the splitting in the case of strong crystal field and weak spin-orbit coupling results from the direct product of the representation of the orbital angular momentum and spin magnetic moment. For the C_{4v} symmetry we have $\mathcal{D}^3(\mathcal{D}^L) = A_2 + B_1 + B_2 + 2E$ and $\mathcal{D}^1(\mathcal{D}^S) = A_2 + E$ which gives 21 states $\mathcal{D}^3 \otimes \mathcal{D}^1 = (A_1 + E) + (B_2 + E) + (B_1 + E) + 2(A_1 + A_2 + B_1 + B_2 + E)$ as shown in Fig. 2. In the case of cubic (O_h) symmetry the orbital and spin moments transform according to $\mathcal{D}^3(\mathcal{D}^L) = \Gamma_2^+ + \Gamma_5^+ + \Gamma_4^+$ and $\mathcal{D}^1(\mathcal{D}^S) = \Gamma_4^+$, respectively, which gives the following splitting of the levels $\mathcal{D}^3 \otimes \mathcal{D}^1 = \Gamma_5^+ + (\Gamma_3^+ + \Gamma_4^+ + \Gamma_5^+ + \Gamma_2^+) + (\Gamma_5^+ + \Gamma_3^+ + \Gamma_4^+ + \Gamma_1^+)$. The spin-orbit coupling does not split the singlet states. For the C_{4v} symmetry we have for the ^1D level $\mathcal{D}^2(\mathcal{D}^L) \otimes \mathcal{D}^0(\mathcal{D}^S) = (A_1 + B_1) + (B_2 + E)$ and for the O_h symmetry $\mathcal{D}^2(\mathcal{D}^L) \otimes \mathcal{D}^0(\mathcal{D}^S) = \Gamma_3^+ + \Gamma_5^+$. However, it shifts their energy due to the admixture of the triplet states. As a consequence some single-triplet transitions become allowed.

2. Fine structure of the NiO(001) surface

Figure 2 (bottom) shows the calculated fine structure of the NiO(001) surface. The energy diagram of the corresponding $3d^8$ levels of the Ni^{2+} ion, which are split by the tetragonal-pyramid crystal field, is reported.

The $^3B_1$ ground state of Ni^{2+} is split by spin-orbit coupling into two levels corresponding to onefold and twofold degeneracies, i.e., 0 and 3.1 meV, respectively. This splitting of the ground state (3.1 meV) between the two lowest-lying fine-structure levels of the NiO(001) surface is large in comparison with typical magnetic anisotropy energies of the bulk systems. Together with the large orbital magnetic moment of NiO it points towards a large magnetic surface anisotropy. We should note that we take the zero level of energy at the lowest energy of these splitting levels. However, this zero-level energy (with spin-orbit interaction) is slightly different from the $^3B_1$ ground state (the zero-level energy without

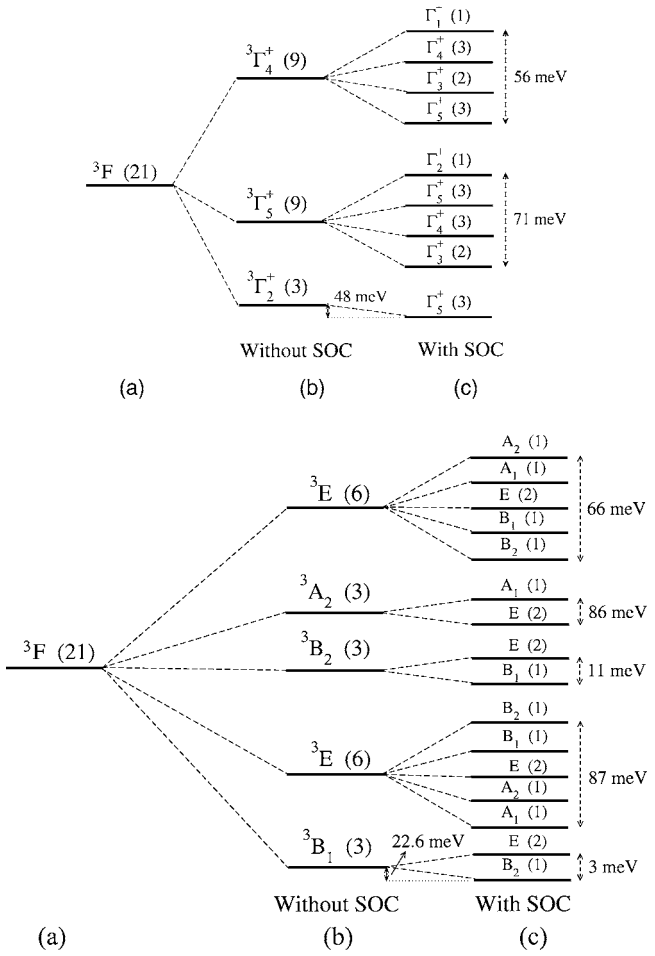

FIG. 2. Symmetry classifications of the electronic states in the point groups O_h and C_{4v} describing the crystal field in the bulk and at the (001) surface of NiO. The degeneracy of each state is given in parentheses. For the symmetry group O_h the irreducible representation of the dipole operator is Γ_4^-. Therefore the allowed dipole transitions are among the states with the change of parity $\Gamma_1^{+/-} \leftrightarrow \Gamma_4^{-/+}$; $\Gamma_2^{+/-} \leftrightarrow \Gamma_5^{-/+}$; $\Gamma_3^{+/-} \leftrightarrow \Gamma_4^{-/+}, \Gamma_5^{-/+}$; $\Gamma_4^{+/-} \leftrightarrow \Gamma_1^{-/+}, \Gamma_3^{-/+}, \Gamma_4^{-/+}, \Gamma_5^{-/+}$; $\Gamma_5^{+/-} \leftrightarrow \Gamma_2^{-/+}, \Gamma_3^{-/+}, \Gamma_4^{-/+}, \Gamma_5^{-/+}$; (and the transitions must change the parity). For C_{4v} symmetry the irreducible representation of the dipole operator is A_1+E. Therefore the only allowed dipole transitions are among the states $A_1 \leftrightarrow A_1, E$; $A_2 \leftrightarrow A_2, E$; $B_1 \leftrightarrow B_1, E$; $B_2 \leftrightarrow B_2, E$; $E \leftrightarrow A_1, A_2, B_1, B_2, E$ (parity is no good quantum number at the surface).

spin-orbit interaction). When spin-orbit interaction is included, the lowest energy equals −22.6 meV compared to the previous $^3B_1$ ground state [see Fig. 2 (bottom)].

The NiO(001) surface has four low-lying excited states, ^3E, $^3B_2$, $^3A_2$, and ^3E, in the C_{4v} crystal field as shown in Fig. 2 (top). The first excited state ^3E is split into six components at about 602.2, 608.5, 647.1, 665.7, and 689.3 meV. These fine structure levels are nondegenerate, except for the third one, which is twofold degenerate. Note that these splitting energies refer to the zero energy as defined above. The energy splittings due to spin-orbit interaction of the second $^3B_2$ excited state belong to three components of single- and double-degeneracies (at values of 1072.5 and 1083.3 meV, respectively). The splitting energy analysis of the third $^3A_2$ excited state shows three components corresponding to double and single degeneracies (2087.4 and 2172.8 meV, respectively). Finally, the six components of the last ^3E excited state are also shown in Fig. 2 (bottom). Five fine structure levels, 2947.2, 2967.5, 2968.9, 3005.9, and 3012.9 meV, are found (the first, second, fourth, and fifth levels are nondegenerate while the third value exhibits a twofold degeneracy).

TABLE I. Energy level scheme of $(NiO_5)^{8-}$ cluster calculation for the (001) surface of NiO. The first column represents the crystal field splitting of the ^3F (21 states) and two lowest singlet states in the absence of spin-orbit coupling. The second column shows the spin-orbit splitting of these states. Corresponding energies (in electron-volts) are given in the third column.

1 $^3B_1$(3)	1	B_2	0.000
	2	E(2)	0.003
	3		0.003
2 ^3E(6)	4	A_1	0.602
	5	A_2	0.609
	6	E(2)	0.647
	7		0.647
	8	B_1	0.666
	9	B_2	0.689
3 $^3B_2$(3)	10	B_1	1.072
	11	E(2)	1.083
	12		1.083
4 $^1A_1$	13	A_1	1.948
5 $^3A_2$(3)	14	E(2)	2.087
	15		2.087
	16	A_1	2.173
6 $^1B_1$	17	B_1	2.293
7 ^3E(6)	18	B_2	2.947
	19	B_1	2.967
	20	E(2)	2.969
	21		2.969
	22	A_1	3.006
	23	A_2	3.013

The splitting energies of all singlet and triplet excited states (only the first 23 excited states) for two systems (with and without the inclusion of spin-orbit interaction) are summarized in Table I.

3. Fine structure of bulk NiO

Figure 2 (top) shows the calculated fine structure of bulk NiO. Correspondingly, Table III displays energy levels of the ground and low-lying excited states. For the comparison with experiment we refer to the optical second harmonic generation data of Ref. 18. It is well known that antiferromagnetic ordering is typical for this transition metal oxide. It is clear that in order to describe this antiferromagnetism by means of the cluster calculation one needs more than one Ni ion in the

model system. However, there are several effects of spin-orbit coupling even in the small cluster we consider. First, its inclusion leads to a slight lowering of the ground state energy $[E_{^3\Gamma_2^+}$ (without SOC)$-E_{\Gamma_5^+}$(with SOC)$=48$ meV]. We should note that the corresponding symmetry of each level is given in Fig. 2 (top). The splitting of the second excited state ($\Delta E_{^3\Gamma_5^+}=E_{\Gamma_2^+}-E_{\Gamma_3^+}=71$ meV) ($^3\Gamma_5^+$) agrees well with the most accurate measurements (around 70 meV) of the optical absorption and second harmonic generation spectra of NiO.[37] However, important differences have been observed. The assignment of the levels to the peaks in the optical absorption spectra from Fiebig *et al.*[18] shows almost equal distances among the sublevels of the $^3\Gamma_5^+$ state. A very narrow splitting of the first sublevel Γ_3^+ of approximately 5.1 meV occurs and is attributed to the exchange field breaking of the symmetry. In contrast, our calculation shows very small distances between the second and the first, and forth and third sublevels (8 and 9 meV respectively). Therefore, we argue that two sharp lines in the optical absorption spectra may also result solely from the spin-orbit coupling rather than from exchange field splitting. In addition, our $^3\Gamma_2^+ \rightarrow {}^3\Gamma_5^+$ transition at about 0.9 eV is in good agreement with the SHG line of 1.0 eV by Fiebig *et al.*[18]

However, the $^3\Gamma_2^+ \rightarrow {}^3\Gamma_4^+$ transition is at a much higher energy of 2.74 eV compared with the experimental observation at about 1.75 eV in Ref. 18. The computation of the second excited state is clearly less precise due to the importance of the correlation effects [QCISD(T) lowers its energy by 0.64 eV compared to CIS]. However, we expect that this should not affect the fine structure of the level much. The experimental resolution does not allow to clearly distinguish among the participating states, and we restrict ourselves to the remark that the broadening of the splitting between the Γ_5^+ and Γ_1^+ sublevels equals 56 meV as shown in Fig. 2 (top). However, the relative position of the sublevels differs from that proposed in the early theoretical work by Ferguson and Guggenheim.[38]

4. Comparison with nonrelativistic approach

In addition, we compare the weighted averages of the spin-orbit split states and the nonrelativistic states. In the bulk case (O_h symmetry) the ^3F level is split due to the crystal field in the absense of spin-orbit interaction into $^3\Gamma_2^+$, $^3\Gamma_5^+$, and $^3\Gamma_4^+$ sublevels with the relative energies of 1.01 and 2.86 eV. Weight average over the spin-orbit split states slightly lifts these values: 1.05 eV for $^3\Gamma_5^+$ and 2.90 eV for $^3\Gamma_4^+$. Averaged energies were shifted in order to match the nonrelativistic ground state energy. Analogously, in the surface case the inclusion of spin-orbit interaction leads to a small lifting of the state-averaged energies in comparison with nonrelativistic energies. The tetragonal-pyramid crystal field splits the ^3F level by 0.62, 1.06, 2.07, and 2.96 eV into $^3B_1$, ^3E, $^3B_2$, $^3A_2$, and ^3E sublevels, while the inclusion of spin-orbit coupling with subsequent averaging leads to the energies of 0.64, 1.08, 2.11, and 2.98 eV, respectively (see Table II).

B. Transition moments

As discussed before, we perform three different types of CI calculations for the NiO surface cluster. On the first step a nonrelativistic CIS calculation by means of the GAUSSIAN 98 package yields the crystal field splitting of the levels and the ED transitions among them. We will only consider the lowest seven levels (in the absence of SOC) that span an energy interval of approximately 3.0 eV. Most of these states are triplets that in the absence of the crystal field join to form the ^3F state. The only two singlets originate from the ^1D level. The corresponding dipole transition matrix elements are shown in Fig. 3(a).

TABLE II. Energy level scheme of $(NiO_6)^{10-}$ cluster calculation for bulk NiO. The first column represents the crystal field splitting of ^3F (21 states) and two lowest singlet states in the absence of spin-orbit coupling. The second column shows a spin-orbit splitting of these states. Corresponding energies (in electron-volts) are given in the third column.

$1\ ^3\Gamma_2^+(3)$	1		0.000
	2	$\Gamma_5^+(3)$	0.000
	3		0.000
$2\ ^3\Gamma_5^+(9)$	4	$\Gamma_3^+(2)$	1.020
	5		1.020
	6		1.028
	7	$\Gamma_4^+(3)$	1.028
	8		1.028
	9		1.082
	10	$\Gamma_5^+(3)$	1.082
	11		1.082
	12	Γ_2^+	1.091
$3\ ^1\Gamma_3^+(2)$	13	$\Gamma_3^+(2)$	2.328
	14		2.328
$4\ ^3\Gamma_4^+(9)$	15		2.868
	16	$\Gamma_5^+(3)$	2.868
	17		2.868
	18	$\Gamma_3^+(2)$	2.894
	19		2.894
	20		2.914
	21	$\Gamma_4^+(3)$	2.914
	22		2.914
	23	Γ_1^+	2.924

On the next stage we use the COLUMBUS program package to perform various relativistic CI calculations. First, we set the valence spin-orbit operators on the Ni^{2+} ion to zero which allows us to reproduce previous GAUSSIAN 98 results revealing the degeneracy of each state. The dipole transitions among the states remain the same as in the prior nonrelativistic calculations implying, however, new selection rules. The placement of nonzero ED matrix elements can be easily conceived from Fig. 3(b).

Last, we place realistic valence spin-orbit operators on the Ni ion revealing the fine structure of the energetic scheme. The degeneracy of each state is significantly lowered due to the presence of spin-orbit coupling. The classification of all 23 states due to the symmetry and their energies are shown

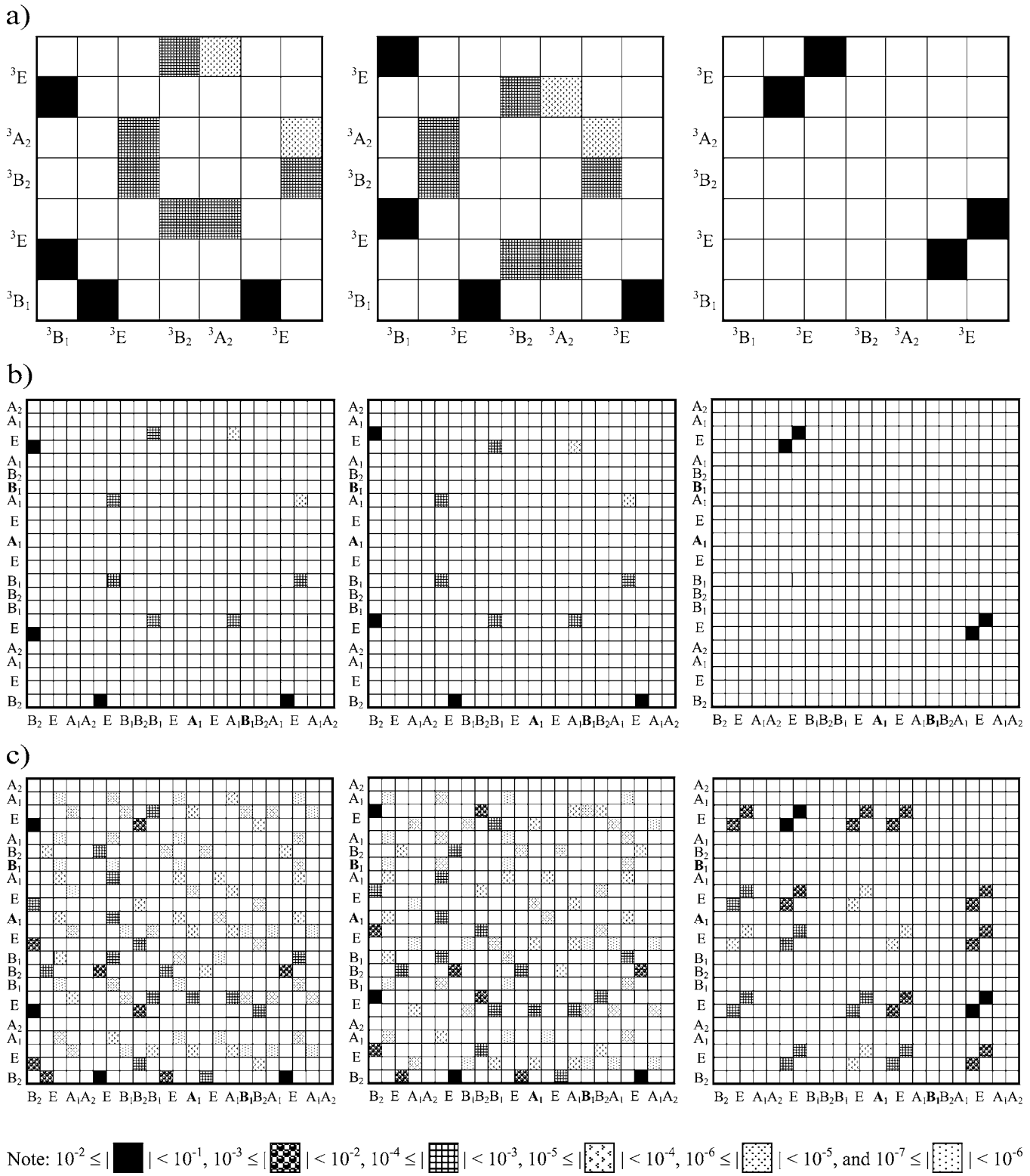

FIG. 3. Electric-dipole transition matrix elements for the (001) surface of NiO on different levels of the theory (in atomic units). (a) Spin-orbit interaction is not taken into account, triplets only, (b) SO-CIS calculation artificially setting SO interaction operators to zero, (c) full-fledged SO calculation. x, y, z projections of the transition dipole moment are shown in the first to the third columns, respectively. Note that the singlet states are printed in bold face for clarity.

in the second and third column of Table I. Comparison of the results of the two last calculations can be done by analyzing the wave-function expansion coefficients. We will outline below how to obtain the ED transition matrix elements among the states. Let us denote states from the nonrelativistic calculation as α,β,γ. We label the states from relativistic calculations by i',j',k' in the absence of SOC and by i,j,k when SOC is already taken into account. The nonzero ED matrix elements $\langle\alpha|\vec{d}|\beta\rangle$ and $\langle i'|\vec{d}|j'\rangle$ are identical for the states from the same irreducible representation. In particular this means

$$\langle i'|\vec{d}|j'\rangle = \langle\alpha|\vec{d}|\beta\rangle \text{ where } i' \in \alpha \times \mathcal{D}^1, \text{ and } j' \in \beta \times \mathcal{D}^1.$$

The ED transitions among i,j,k states can than be expressed the via overlap matrix $\langle i|i'\rangle$ as

$$\langle i|\vec{d}|j\rangle = \sum_{i'}\sum_{j'}\langle i|i'\rangle\langle i'|\vec{d}|j'\rangle\langle j'|j\rangle. \tag{8}$$

The overlap matrix for the NiO (001) surface has a block-diagonal structure, each block $\mathcal{L}$ of nonzero elements corresponding to the irreducible representations, in our case A_1, A_2, B_1, B_2, E,

$$\langle i|i'\rangle = \text{diag}[\mathcal{L}(A_1),\mathcal{L}(A_2),\mathcal{L}(B_1),\mathcal{L}(B_2),\mathcal{L}(E)]. \tag{9}$$

The numerical values of the overlap are given by matrices Eqs. (10)–(14) respectively

$$\mathcal{L}(A_1) = \begin{pmatrix} & 4 & 13 & 16 & 22 \\ 4 & 0.998 & -0.029 & 0.061 & -0.009 \\ 13 & 0.054 & 0.883 & -0.465 & 0.026 \\ 16 & -0.040 & 0.467 & 0.883 & 0.007 \\ 22 & 0.008 & -0.026 & 0.006 & 1.000 \end{pmatrix}, \tag{10}$$

$$\mathcal{L}(A_2) = \begin{pmatrix} & 5 & 23 \\ 5 & 1.000 & -0.009 \\ 23 & 0.009 & 1.000 \end{pmatrix}, \tag{11}$$

$$\mathcal{L}(B_1) = \begin{pmatrix} & 8 & 10 & 17 & 19 \\ 8 & 0.997 & 0.063 & 0.044 & -0.008 \\ 10 & -0.061 & 0.996 & -0.059 & -0.029 \\ 17 & -0.046 & 0.060 & 0.987 & 0.129 \\ 19 & 0.012 & 0.022 & -0.130 & 0.991 \end{pmatrix}, \tag{12}$$

$$\mathcal{L}(B_2) = \begin{pmatrix} & 1 & 9 & 18 \\ 1 & 0.989 & 0.147 & -0.004 \\ 9 & -0.147 & 0.989 & 0.012 \\ 18 & 0.006 & -0.011 & 1.000 \end{pmatrix}, \tag{13}$$

$$\mathcal{L}(E) = \begin{pmatrix} & 2\|3 & 6\|7 & 11\|12 & 14\|15 & 20\|21 \\ 2\|3 & 0.992 & 0.105 & -0.076 & -0.002 & 0.019 \\ 6\|7 & -0.109 & 0.993 & -0.045 & -0.026 & -0.007 \\ 11\|12 & 0.070 & 0.054 & 0.994 & -0.006 & -0.011 \\ 14\|15 & -0.005 & 0.022 & -0.065 & 0.997 & -0.026 \\ 20\|21 & -0.002 & 0.008 & 0.009 & 0.027 & 1.000 \end{pmatrix}. \tag{14}$$

TABLE III. Energy level scheme of $(NiO_5)^{8-}$ cluster calculation of the (001) surface of NiO. The state number in the first column corresponds to the level designation of the fine structure splitting. The states without the labeled state number in the table are the low-lying excited states excluding the SOC effect.

State number	State	Composition percentage	ΔE (eV)
1	B_2	$^3B_1$:97.8, 1^3E:2.2	0.000
2|3	E	$^3B_1$:98.4, 1^3E:1.2	0.003
	$^3B_1$		0.023
4	A_1	1^3E:99.6, $^1A_1$:0.3, $^3A_2$:0.2	0.602
5	A_2	1^3E:100.0	0.609
6|7	E	1^3E:98.6, $^3B_1$:1.1, $^3B_2$:0.3	0.647
8	B_1	1^3E:99.4, $^3B_2$:0.4, $^1B_1$:0.2	0.666
9	B_2	1^3E:97.8, $^3B_1$:2.2	0.689
	^3E		0.641
10	B_1	$^3B_2$:99.2, 1^3E:0.4, $^1B_1$:0.4	1.072
11|12	E	$^3B_2$:99.8, $^3B_1$:0.6, 1^3E:0.2, $^3A_2$:0.4	1.083
	$^3B_2$		1.078
13	A_1	$^1A_1$:78.0, $^3A_2$:21.8	1.948
	$^1A_1$		2.031
14|15	E	$^3A_2$:99.4	2.087
16	A_1	$^3A_2$:78.0, $^1A_1$:21.6, 1^3E:0.4	2.173
	$^3A_2$		2.089
17	B_1	$^1B_1$:97.4, $2E^3$:1.7, $^3B_2$:0.3, 1^3E:0.2	2.293
	$^1B_1$		2.302
18	B_2	2^3E:100.0	2.947
19	B_1	2^3E:98.2, $^1B_1$:1.7	2.947
20|21	E	2^3E:100.0	2.969
22	A_1	2^3E:100.0, $^1A_1$:0.1	3.006
23	A_2	2^3E:100.0	3.013
	^3E		2.983

Numbers denoting rows (i') and columns (i) are that given in Table I. The matrices are unitary. This reflects the normalization and orthogonality of the wave functions i' and i. Overlap matrix elements between wave functions from different irreducible representations are always zero. The magnitude of the matrix elements is an important quantity that shows how strong levels mix due to spin-orbit coupling (Table III). In particular, one sees that the A_1 level from the fine structure splitting of the $^3A_2$ state gets a strong admixture between the triplet and the singlet states:[39] $(16A_1) \approx (^3A_2)^{0.78}(^1A_1)^{0.22}$ accompanying the substantial splitting of the $^3A_2$ level (86 meV). On the other hand the sublevels of the $^3B_1$ ground state are not substantially influenced by spin-orbit coupling $[(1B_2) \approx (^3B_1)^{0.99}(^3E)^{0.02}]$, since the largest percentage in the composition of a level corresponds to the purity of the level in the coupling scheme. In this coupling scheme, there is very little mixing with the other spin-state yielding the negligible splitting of 3 meV. The energy splittings of other states could likewise be explained from the nature of their mixing with other spin states. It is to be noted further that, as consequence of such mixing the transition probability between the singlet and triplet states can be assisted through the spin-orbit mixing of different states (third row of Fig. 3). The matrices of electric dipole transitions have been obtained according to Eq. (8) combining together matrix elements of electric-dipole transitions in the absence of SO coupling with the overlap.

IV. CONCLUSIONS

We have studied the effects of spin-orbit interaction on the low-lying excited states by means of *ab initio* theory. In particular, we have found additional transition electric-dipole moments, for detecting a SHG signal from the NiO(001) surface within the electric-dipole approximation, for which spin-orbit coupling is included. It is shown that the splitting of energies leads to additional ED transitions, which correspond to SHG response that can be observed when SOC is taken into account.

ACKNOWLEDGMENTS

This work has been supported by the DFG-Schwerpunktprogramme (SPP 1133 and SPP 1153), by the EU RTN-networks EXCITING and DYNAMICS, as well as by Landesschwerpunkt MINAS.

[1] A. V. Soudackov, A. L. Tchougreeff, and I. A. Misurkin, Int. J. Quantum Chem. **58**, 161 (1996).
[2] O. Laporte, Z. Phys. **47**, 761 (1928).
[3] R. Newman and R. M. Chrenko, Phys. Rev. **114**, 1507 (1959).
[4] A. Freitag, V. Staemmler, D. Cappus, C. A. V. K. Al-Shamery, Jr., H. Kuhlenbeck, and H.-J. Freund, Chem. Phys. Lett. **210**, 10 (1993).
[5] A. Gorschlüter and H. Merz, Phys. Rev. B **49**, 17293 (1994).
[6] B. Fromme, M. Schmitt, E. Kisker, A. Gorschlüter, and H. Merz, Phys. Rev. B **50**, 1874 (1994).
[7] B. Fromme, A. Hylla, C. Koch, E. Kisker, A. Gorschlüter, and H. Merz, J. Magn. Magn. Mater. **148**, 181 (1995).
[8] B. Fromme, C. Koch, R. Deussen, and E. Kisker, Phys. Rev. Lett. **75**, 693 (1995).
[9] B. Fromme, M. Möller, T. Anschütz, C. Bethke, and E. Kisker, Phys. Rev. Lett. **77**, 1548 (1996).
[10] B. Fromme, Springer Tracts Mod. Phys. **170**, 1 (2001).
[11] D. Reinen and B. Bunsenges, J. Phys. Chem. **69**, 82 (1965).
[12] B. D. Bird, G. A. Osborne, and P. J. Stephens, Phys. Rev. B **5**, 1800 (1972).
[13] M. Belkhir and J. Hugel, Solid State Commun. **70**, 471 (1989).
[14] W. C. Mackrodt and C. Noguera, Surf. Sci. **457**, L386 (2000).
[15] C. de Graaf, R. Broer, and W. C. Nieuwpoort, Chem. Phys. Lett. **208**, 35 (1996).
[16] M. Geleijns, C. de Graaf, R. Broer, and W. C. Nieuwpoort, Surf. Sci. **421**, 106 (1999).

[17] K. Satitkovitchai, Y. Pavlyukh, and W. Hübner, Phys. Rev. B **67**, 165413 (2003).
[18] M. Fiebig, D. Fröhlich, T. Lottermoser, V. V. Pavlov, R. V. Pisarev, and H.-J. Weber, Phys. Rev. Lett. **87**, 137202 (2001).
[19] J. H. V. Vleck, Phys. Rev. **52**, 1178 (1937).
[20] H. Brooks, Phys. Rev. **58**, 909 (1940).
[21] Note that for all calculations performed with the COLUMBUS quantum chemistry program, the lower symmetry C_{2v} is used instead of the higher symmetry C_{4v}, after having generated the input files, according to Pitzer's theorem. This theorem states that atomic orbital integrals related by symmetry contribute equally to symmetry orbital integrals whose integrands are totally symmetric.
[22] R. W. G. Wyckoff, *Crystal Structures* (Interscience, New York, 1964).
[23] P. J. Hay and W. R. Wadt, J. Chem. Phys. **82**, 284 (1985).
[24] M. Francl, W. Petro, W. Hehre, J. Binkley, M. Gordon, D. DeFrees, and J. Pople, J. Chem. Phys. **77**, 3654 (1982).
[25] P. S. T. Clark and J. Chandrasekhar, J. Comput. Chem. **4**, 294 (1983).
[26] R. Krishnam, J. Binkley, R. Seeger, and J. Pople, J. Chem. Phys. **72**, 650 (1980).
[27] S. Yabushita, Z. Zhang, and R. M. Pitzer, J. Phys. Chem. A **103**, 5791 (1999).
[28] R. M. Pitzer and N. W. Winter, Int. J. Quantum Chem. **40**, 773 (1991).
[29] H. Lischka, R. Shepard, F. B. Brown, and I. Shavitt, Int. J. Quantum Chem., Quantum Chem. Symp. **15**, 91 (1981).
[30] R. Shepard, I. Shavitt, R. M. Pitzer, D. C. Comeau, M. Pepper, H. Lischka, P. G. Szalay, R. Ahlrichs, F. B. Brown, and J. Zhao, Int. J. Quantum Chem., Quantum Chem. Symp. **22**, 149 (1988).
[31] H. Lischka, R. Shepard, R. M. Pitzer, I. Shavitt, M. Dallos, T. Müller, P. G. Szalay, M. Seth, G. S. Kedziora, S. Yabushita, and Z. Zhang, Phys. Chem. Chem. Phys. **3**, 664 (2001).
[32] H. Lischka, R. Shepard, I. Shavitt, R. M. Pitzer, M. Dallos, T. Müller, P. G. Szalay, F. B. Brown, R. Ahlrichs, H. J. Böhm, A. Chang, D. C. Comeau, R. Gdantiz, H. Dachsel, C. Ehrhardt, M. Ernzerhof, P. Höchtl, S. Irle, G. Kidziora, T. Kovar, V. Parasuk, M. J. M. Pepper, P. Scharf, H. Schiffer, M. Schindler, M. Schüler, M. Seth, E. A. Stahlberg, J.-G. Zhao, S. Yabushita, and Z. Zhang, COLUMBUS, an *ab initio* electronic structure program, release 5.8 (2001).
[33] R. B. Ross, W. C. Ermler, and P. A. Christiansen, J. Chem. Phys. **84**, 3297 (1986).
[34] R. M. Pitzer and N. W. Winter, J. Phys. Chem. **92**, 3061 (1988).
[35] P. Hafner and W. H. E. Schwarz, Chem. Phys. Lett. **65**, 537 (1979).
[36] A. P. Cracknell, Adv. Phys. **17**, 367 (1968).
[37] The spin-orbit splitting of the $^3\Gamma_5^+$ excited state has been clearly resolved by the optical absorption as well as by the second harmonic generation experiments Figs. 1(a), 1(b) of Ref. 18. The spectra recorded in the energy interval of 0.80–1.15 eV show several well pronounced peaks with energies of 0.975, 1.000, 1.025, and 1.050 eV. In this experimental work they were assigned to sublevels Γ_3^+, Γ_4^+, Γ_5^+, and Γ_2^+. It was argued that the two lowest sharp lines in the SH spectrum with energies of 0.9685 and 0.9736 eV result from the exchange field splitting of Γ_3^+ level. In our work the splitting sublevel energies of $^3\Gamma_5^+$ comprise 1.020, 1.028, 1.082, and 1.091 eV for Γ_3^+, Γ_4^+, Γ_5^+, and Γ_2^+, respectively.
[38] J. Ferguson and H. J. Guggenheim, J. Chem. Phys. **44**, 1095 (1966).
[39] It is important to notice that the energy splitting and mixing of levels strongly depend on their energy separation. The CIS method places the $^3A_2$ level at higher energy compared to experiment. We therefore expect that by using a more sophisticated computational scheme its energy separation from the $^3B_2$ level will be reduced leading to a stronger SO mixing between these levels, while reducing the mixing with the $^1A_1$ state.